Nanoscale Research Letters
a SpringerOpen Journal

NANO EXPRESS Open Access

Effects of post-deposition annealing ambient on band alignment of RF magnetron-sputtered Y_2O_3 film on gallium nitride

Hock Jin Quah and Kuan Yew Cheong*

Abstract

The effects of different post-deposition annealing ambients (oxygen, argon, forming gas (95% N_2 + 5% H_2), and nitrogen) on radio frequency magnetron-sputtered yttrium oxide (Y_2O_3) films on n-type gallium nitride (GaN) substrate were studied in this work. X-ray photoelectron spectroscopy was utilized to extract the bandgap of Y_2O_3 and interfacial layer as well as establishing the energy band alignment of Y_2O_3/interfacial layer/GaN structure. Three different structures of energy band alignment were obtained, and the change of band alignment influenced leakage current density-electrical breakdown field characteristics of the samples subjected to different post-deposition annealing ambients. Of these investigated samples, ability of the sample annealed in O_2 ambient to withstand the highest electric breakdown field (approximately 6.6 MV/cm) at 10^{-6} A/cm^2 was related to the largest conduction band offset of interfacial layer/GaN (3.77 eV) and barrier height (3.72 eV).

Keywords: Yttrium oxide, Gallium nitride, Post-deposition annealing, Band alignment, Conduction band offset

Background

Increasing concerns regarding the escalating demand of energy consumption throughout the world has triggered the needs of developing energy-efficient high-power and high-temperature metal-oxide-semiconductor (MOS)-based devices. It has been projected that gallium nitride (GaN) has the potential of conforming to the needs of these MOS-based devices due to its promising properties, which include wide bandgap (3.4 eV), large critical electric field (3 MV/cm), high electron mobility, as well as good thermal conductivity and stability [1-6]. The fabrication of a functional GaN-based MOS device requires a high-quality gate oxide that is capable of resisting a high transverse electric field [7,8]. Native oxide (Ga_2O_3) of GaN [9-13] and a relatively low-dielectric-constant (k) SiN_xO_y [2] or SiO_2 [14-19] have been successfully grown and deposited, respectively, as gate oxides in GaN-based MOS devices. However, these gate oxides are not the preferred choices. The shortcoming encountered by the former gate is the slow growth gate, high oxidation temperature (>700°C), and high leakage current [12,13] while the latter gate with a relatively low k is unable to withstand the high electric field imposed on GaN [7,20,21]. Thereafter, numerous high-k gate oxides [3,20-28] have been selected for investigation on GaN-based MOS devices. Recent exploration on the employment of radio frequency (RF) magnetron-sputtered Y_2O_3 gate subjected to post-deposition annealing (PDA) from 200°C to 1,000°C for 30 min in argon ambient has revealed that the Y_2O_3 gate annealed at 400°C has yielded the best current density-breakdown field (J-E) characteristic as well as the lowest effective oxide charge, interface trap density, and total interface trap density [25]. It is noticed that the acquired J-E characteristic for this sample is better than majority of the investigated gate oxide materials [25]. The ability of Y_2O_3/GaN MOS structure to be driven at a high E and low J is attributed to the fascinating properties possessed by Y_2O_3, such as high k value (k = 12 to 18), large bandgap (approximately 5.5 eV), and large conduction band offset (approximately 1.97 eV) [25,29-31]. Despite that, the presence of oxygen-related defects, changes in compositional homogeneity of Y_2O_3, and formation of interfacial layer (IL) are of particular concern as

* Correspondence: cheong@eng.usm.my
Energy Efficient & Sustainable Semiconductor Research Group, School of Materials and Mineral Resources Engineering, Universiti Sains Malaysia, Engineering Campus, Nibong Tebal, Seberang Perai Selatan, Penang 14300, Malaysia

either of these factors might alter the bandgap of Y_2O_3 and band alignment of Y_2O_3 with respect to the GaN, which would influence the *J-E* characteristic of the MOS structure. Li et al. has reported previously that *J-E* characteristic of the MOS structure is dependent on the thickness of IL, wherein interface quality of the atomic layer deposited HfO_2 on Si can be altered via the IL thickness [32]. In order to reduce oxygen-related defects and restore compositional homogeneity of Y_2O_3, it is essential to perform post-deposition annealing on the oxide [33]. Besides, the oxygen content near the Y_2O_3/GaN interface can be regulated by varying the post-deposition annealing ambient and eventually controlling the formation of IL. Therefore, engineering of the bandgap of Y_2O_3 gate and band alignment of Y_2O_3 with GaN through different PDA ambients is of technological importance. In this work, effects of different PDA ambients (oxygen (O_2), argon (Ar) [25], nitrogen (N_2), and forming gas (FG; 95% N_2 + 5% H_2)) at 400°C for 30 min on the Y_2O_3/GaN structure in modifying the bandgap of Y_2O_3 gate and band alignment of Y_2O_3/GaN are presented. A correlation on the bandgap of Y_2O_3 gate and band alignment of Y_2O_3/GaN with regard to the *J-E* characteristics is also discussed in this paper.

Methods

Prior to the deposition of 60-nm thick Y_2O_3 films on the commercially purchased Si-doped (n-type) GaN epitaxial layers with thickness of 7 μm and doping concentration of 1 to 9 × 10^{18} cm^{-3} grown on sapphire substrates, the wafer, which was diced into smaller pieces, were subjected to RCA cleaning. Subsequently, these samples were loaded into a vacuum chamber of RF magnetron sputtering system (Edwards A500, Edwards, Sanborn, NY, USA). A comprehensive description on the deposition process of Y_2O_3 films has been reported elsewhere [29,30]. Then, PDA was performed in a horizontal tube furnace at 400°C in different ambients (O_2, Ar, N_2, and FG (95%N_2 + 5% H_2)) for 30 min. The heating and cooling rate of approximately 10°C/min was used for the PDA process. After the PDA process, X-ray photoelectron spectroscopy (XPS) measurements were conducted on the samples at the Research Center for Surface and Materials Science, Auckland University, New Zealand, using Kratos Axis Ultra DLD (Shimadzu, Kyoto, Japan) equipped with a monochromatic Al-K_α X-ray source ($h\nu$ = 1486.69 eV). The spectra of the survey scan were obtained at a low pass energy of 160 eV with an energy resolution of 0.1 eV, and the photoelectron take-off angle was fixed at 0° with respect to the surface normal. Chemical depth profiling was performed by etching the samples using an Ar ion gun operated at 5 keV in order to identify the boundary of Y_2O_3 and interfacial layer between the oxide and GaN. To further determine the bandgap of Y_2O_3 and IL, a detailed scan of O 1*s* was first performed at the same pass energy of 20 eV with an energy resolution of 1.0 eV. The energy loss spectrum of O 1*s* would provide the bandgap of Y_2O_3 and IL by taking into consideration the onset of a single particle excitation and band-to-band transition. Kraut's method was utilized in the extraction of the valence band offset of Y_2O_3 and IL [34,35]. In order to fabricate MOS test structure, the Y_2O_3 film was selectively etched using HF/H_2O (1:1) solution. Next, a blanket of aluminum was evaporated on the Y_2O_3 film using a thermal evaporator (AUTO 306, Edwards). Lastly, an array of Al gate electrode (area = 2.5 × 10^{-3} cm^2) was defined using photolithography process. Figure 1 shows the fabricated Al/Y_2O_3/GaN-based MOS test structure. The current–voltage characteristics of the samples were measured using a computer-controlled semiconductor parameter analyzer (Agilent 4156C, Agilent Technologies, Santa Clara, CA, USA).

Results and discussion

Bandgap (E_g) values for Y_2O_3 and IL are extracted from the onset of the respective energy loss spectrum of O 1*s* core level peaks. The determination of E_g values for Y_2O_3 and IL is done using a linear extrapolation method, wherein the segment of maximum negative slope is extrapolated to the background level [36]. Figure 2a shows typical O 1*s* energy loss spectra of Y_2O_3 and IL for the sample annealed in O_2 ambient. The extracted E_g values are in the range of 4.07 to 4.97 eV and 1.17 to 3.93 eV with a tolerance of 0.05 eV for Y_2O_3 and IL, respectively, for samples annealed in different post-deposition annealing ambients (Figure 3a).

Typical valence band photoelectron spectra of Y_2O_3 and IL for the sample annealed in O_2 ambient are presented in Figure 2b. By means of linear extrapolation method, the valence band edges (E_v) of Y_2O_3 and IL could be determined by extrapolating the maximum negative slope to the minimum horizontal baseline [36]. The acquired valence band offset (ΔE_v) values of

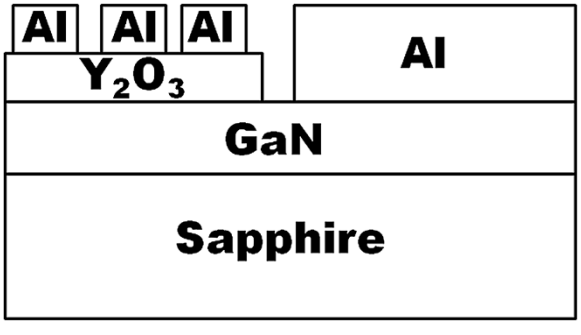

Figure 1 Al/Y_2O_3/GaN MOS test structure.

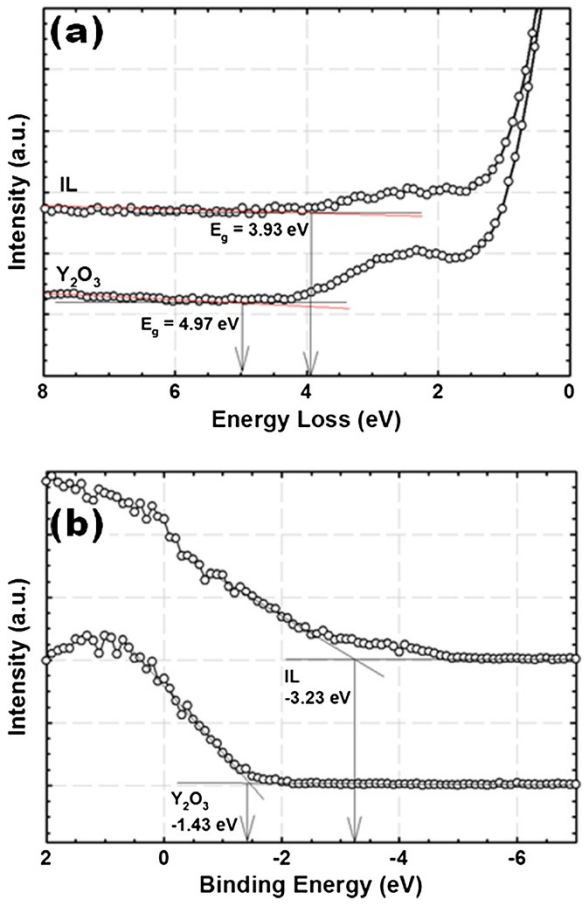

Figure 2 XPS O 1*s* energy loss and valence band photoelectron spectrum. (**a**) Typical XPS O 1*s* energy loss spectrum of Y_2O_3 and interfacial layer for the sample annealed in O_2 ambient. (**b**) Typical valence band spectrum of Y_2O_3 and interfacial layer for the sample annealed in O_2 ambient.

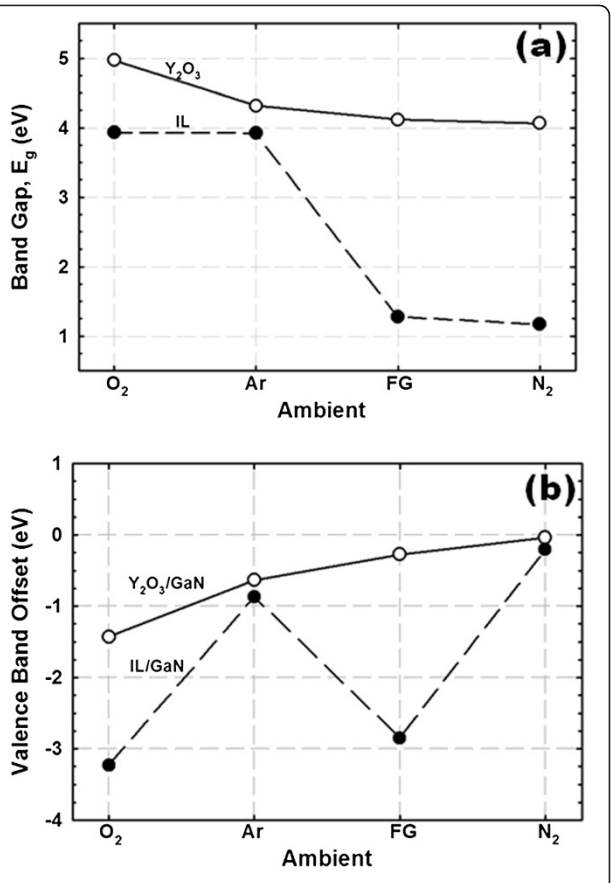

Figure 3 Bandgap and valence band offset of Y_2O_3 and interfacial layer. (**a**) Bandgap of Y_2O_3 and IL for the sample annealed in different ambients. (**b**) Valence band offset of Y_2O_3/GaN and IL/GaN as a function of post-deposition annealing ambient.

Y_2O_3 and IL with respect to GaN substrate are in the range of −0.04 to −1.43 eV and −0.21 to −3.23 eV with a tolerance of 0.05 eV, respectively, for all of the investigated samples. The ΔE_v values of Y_2O_3/GaN and IL/GaN are shown in Figure 3b as a function of PDA ambient.

The determination of both E_g of Y_2O_3 and IL as well as ΔE_v of Y_2O_3/GaN and IL/GaN enables the calculation of the conduction band offset (ΔE_c) of Y_2O_3/GaN, IL/GaN, and Y_2O_3/IL using the following equation: ΔE_c(oxide or IL) = E_g(oxide or IL) − ΔE_v(oxide/GaN or IL/GaN) − E_g (GaN), where $E_{g(GaN)}$ is 3.40 eV for GaN [37]. The obtained values of $\Delta E_c(Y_2O_3/GaN)$, ΔE_c(IL/GaN), and $\Delta E_c(Y_2O_3/IL)$ for all of the investigated samples are presented in Figure 4. In general, a reduction in $E_g(Y_2O_3)$, E_g (IL), $\Delta E_c(Y_2O_3/GaN)$, and ΔE_c(IL/GaN) is observed when different PDA ambients are performed, as indicated by O_2 > Ar > FG > N_2. The IL has been proven using XPS to be comprised of a mixture of Ga-O, Ga-O-N, Y-O, and Y-N bonding (HJQ and KYC, unpublished work). The detection of Ga-O and Ga-O-N bonding in the region of IL indicates that the oxygen dissociated from Y_2O_3 during PDA in different ambients would diffuse inward to react with the decomposed GaN substrate. During PDA in O_2 ambient, an additional source of oxygen from the gas ambient has contributed to the formation of Ga-O

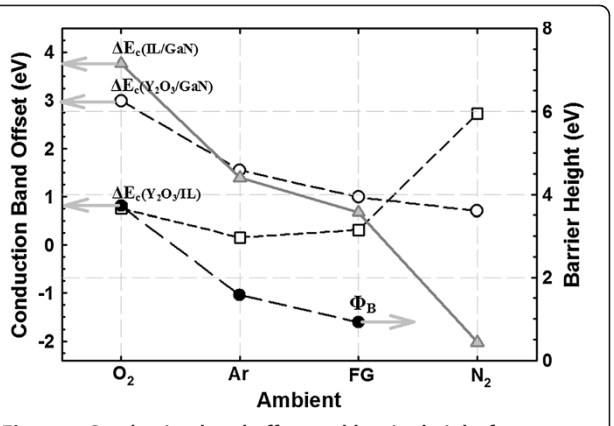

Figure 4 Conduction band offset and barrier height for samples annealed in different ambients.

and Ga-O-N bonding in the region of IL. Sample subjected to PDA in O_2 ambient attains the largest $E_g(Y_2O_3)$ and E_g(IL) as well as the highest values of $\Delta E_c(Y_2O_3/GaN)$ and ΔE_c(IL/GaN). This is related to the supply of O_2 from the gas ambient during PDA, which has contributed to the reduction of oxygen-related defects in the Y_2O_3 film and the improvement in the compositional homogeneity of the oxide film. The absence of O_2 supply during PDA in Ar (inert) and reducing ambient, such as FG and N_2, may be the reason contributing to the attainment of lower $E_g(Y_2O_3)$, E_g(IL), $\Delta E_c(Y_2O_3/GaN)$, and ΔE_c (IL/GaN) values than the sample annealed in O_2. The presence of N_2 in both FG and N_2 ambient has caused the formation of O_2-deficient Y_2O_3 film, wherein N atoms dissociated from N_2 gas may couple with the oxygen-related defects in the Y_2O_3 film [30,38]. In addition, the presence of N_2 in both FG and N_2 ambient is also capable of performing nitridation process to diminish the tendency of O_2 dissociated from the Y_2O_3 film during PDA to diffuse inward and react with the GaN substrate [30]. Thus, the interfacial layer formed in between the Y_2O_3/GaN structure for these samples could be O_2 deficient. Despite the fact that FG and N_2 ambient are capable of providing nitridation and coupling process, the percentage of N_2 in FG ambient (95% N_2) is lower than that in pure N_2. Hence, PDA in N_2 ambient will enhance the nitridation process and coupling of N atoms with the oxygen-related defects in Y_2O_3, which leads to the formation of more O_2-deficient Y_2O_3 film and IL when compared with the sample annealed in FG ambient. This could be the reason leading to the attainment of the lowest $E_g(Y_2O_3)$, E_g(IL), $\Delta E_c(Y_2O_3/GaN)$, and ΔE_c(IL/GaN) values for the sample annealed in N_2 ambient.

A schematic illustration of the energy band alignment of the Y_2O_3/IL/GaN structure that had been subjected to different PDA ambients is presented in Figure 5. Three different energy band alignment structures were obtained due to the effect of PDA ambient. It is noticed that the conduction band edge of IL is higher than that of Y_2O_3 for the sample annealed in O_2 ambient, but it is lower in samples annealed in Ar, FG, and N_2 ambient. This band alignment shift would influence the leakage current density-electrical field (*J-E*) characteristics of the samples (Figure 6). The dielectric breakdown field (E_B) is defined as the electric field that causes a leakage current density of 10^{-6} A/cm^2, which is not related to a permanent oxide breakdown but representing a safe value for device operation [39]. Of all the investigated samples, the sample annealed in O_2 ambient demonstrates the lowest *J* and the highest E_B (approximately 6.6 MV/cm) at *J* of 10^{-6} A/cm^2. This might be attributed to the attainment of the largest $E_g(Y_2O_3)$ and E_g(IL) as well as

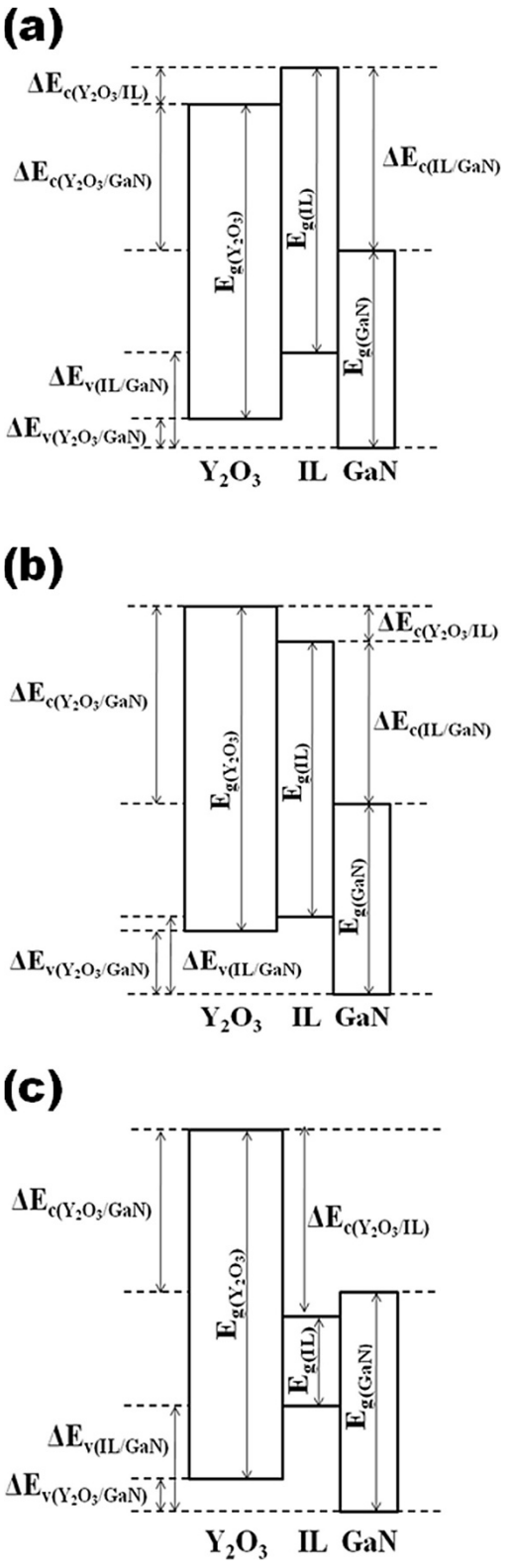

Figure 5 Schematic diagram showing the energy band alignment of the Y_2O_3/IL/GaN system. Energy band alignment of the Y_2O_3/IL/GaN system for the sample annealed in (**a**) oxygen, (**b**) argon and forming gas, and (**c**) nitrogen ambient.

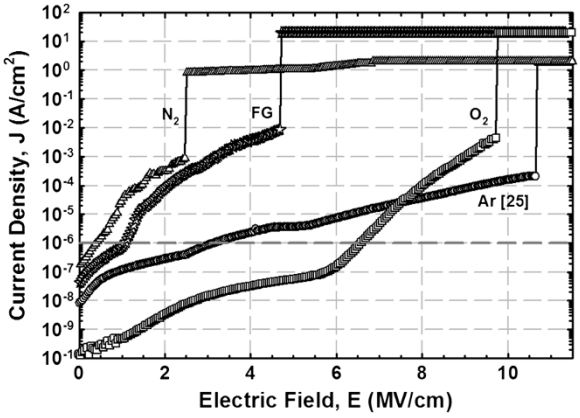

Figure 6 Comparison of *J-E* characteristics of Al/Y_2O_3/IL/GaN-based MOS capacitors.

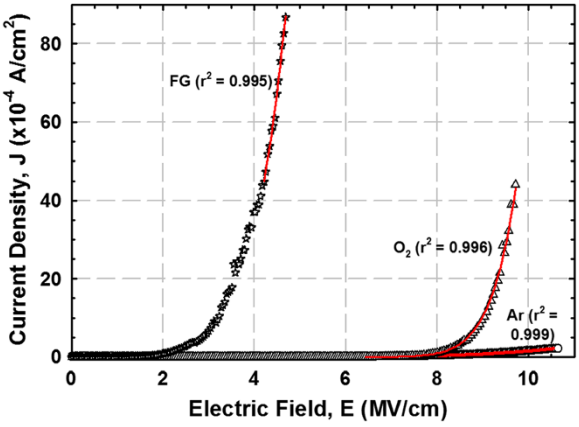

Figure 7 Experimental data fitted well with FN tunneling model. Experimental data (symbol) of samples annealed in O_2, Ar (HJQ and KYC, unpublished work), and FG ambient fitted well with FN tunneling model (line).

the highest values of $\Delta E_c(Y_2O_3/GaN)$ and $\Delta E_c(IL/GaN)$, while for other samples, a deterioration in J and E_B is perceived. The reduction is ranked as Ar > FG > N_2.

In order to determine whether the E_B of the investigated samples is either dominated by the breakdown of IL, Y_2O_3, or a combination of both Y_2O_3 and IL, Fowler-Nordheim (FN) tunneling model is employed to the extract barrier height (Φ_B) of Y_2O_3 on GaN. FN tunneling mechanism is defined as tunneling of the injected charged carrier into the conduction band of the Y_2O_3 gate oxide via passing through a triangular energy barrier [7,8,30]. This mechanism can be expressed as $J_{FN} = AE^2\exp(-B/E)$, where $A = q^3m_o/8(hm\Phi_B$, $B = 4(2\ m)^{1/2}\ \Phi_B^{3/2}/(3qh/2)$, q is the electronic charge, m is the effective electron mass in the Y_2O_3 ($m = 0.1m_o$, where m_o is the free electron mass), and h is Planck's constant [8,40]. In order to fit the obtained experimental data with the FN tunneling model, linear curve fitting method has been normally utilized [8,20,41]. Nevertheless, data transformation is needed in this method owing to the limited models that can be presented in linear forms. Hence, nonlinear curve fitting method is employed using Datafit version 9.0.59 to fit the acquired *J-E* results in this work with the FN tunneling model. It is believed that the extracted results using nonlinear curve fitting method is more accurate due to the utilization of actual data and the minimization of data transformation steps required in the linear curve fitting [42,43]. Figure 7 shows the *J-E* results for the samples annealed in O_2, Ar, and FG ambient, which fitted well with FN tunneling model. The extracted Φ_B values of these samples are presented in the Figure 4. The highest Φ_B value attained by the sample annealed in O_2 ambient (3.72 eV) was higher than that of metal-organic decomposed CeO_2 (1.13 eV) spin-coated on n-type GaN substrate [20]. No Φ_B value has been extracted for the sample annealed in N_2 ambient due to the low E_B and high J of this sample, wherein the gate oxide breaks down prior to the FN tunneling mechanism.

Table 1 compares the computed ΔE_c values from the XPS characterization with the Φ_B value extracted from the FN tunneling model. From this table, it is distinguished that the E_B of the sample annealed in O_2 ambient is dominated by the breakdown of IL as the obtained value of Φ_B from the FN tunneling model is comparable with the value of ΔE_c(IL/GaN) computed from the XPS measurement. For samples annealed in Ar and FG ambient, the acquisition of Φ_B value that is comparable to the $\Delta E_c(Y_2O_3/GaN)$ indicates that the E_B of these samples is actually dominated by the breakdown of bulk Y_2O_3. Since the leakage current of the sample annealed in N_2 ambient is not governed by FN tunneling mechanism, a conclusion in determining whether the E_B of this sample is dominated by the breakdown of IL, Y_2O_3, or a combination of both cannot be deduced. Based on the obtained values of $\Delta E_c(Y_2O_3/GaN)$, ΔE_c(IL/GaN), and $\Delta E_c(Y_2O_3/IL)$, the E_B of this sample is unlikely to be dominated by IL due to the acquisition of a negative ΔE_c (IL/GaN) value for this sample. Thus, the E_B of this sample is most plausible to be dominated by either Y_2O_3 or

Table 1 Comparison of the obtained ΔE_c and Φ_B values

	XPS: conduction band offset			*J-E*
	Y_2O_3/GaN	IL/GaN	Y_2O_3/IL	Barrier height
O_2	3.00	3.77	0.77	3.72
Ar	1.55	1.40	0.15	1.58
FG	0.99	0.68	0.31	0.92
N_2	0.70	−2.03	2.73	[a]

[a]Not influenced by FN tunneling. Therefore, barrier height is not extracted from the FN tunneling model.

a combination of Y_2O_3 and IL. However, the attainment of $\Delta E_c(Y_2O_3/IL)$ value which is larger than that of ΔE_c (Y_2O_3/GaN) value obtained for the samples annealed in Ar and FG ambient eliminates the latter possibility. The reason behind it is if the E_B of the sample annealed in N_2 ambient is dominated by the combination of Y_2O_3 and IL, this sample should be able to sustain a higher E_B and a lower J than the samples annealed in Ar and FG ambient. Therefore, the E_B of the sample annealed in N_2 ambient is most likely dominated by the breakdown of bulk Y_2O_3.

Conclusions

In conclusion, three different energy band alignment models of Y_2O_3/interfacial layer/GaN structure subjected to post-deposition annealing at 400°C in different ambients (O_2, Ar, forming gas (95% N_2 + 5% H_2), and N_2) have been established using X-ray photoelectron spectroscopy. It was proven that the dielectric breakdown field (E_B) of the sample annealed in O_2 ambient was dominated by the breakdown of IL, while the E_B of the samples annealed in Ar, FG, and N_2 ambient was dominated by the breakdown of bulk Y_2O_3. The sample annealed in O_2 ambient demonstrated the best leakage current density-breakdown field due to the attainment of the largest bandgap, the largest conduction band offset, and the highest barrier height value.

Competing interests

The authors declare that they have no competing interests.

Authors' contributions

HJQ carried out all of the experimental work, data analysis of the obtained experimental results, and drafting of the manuscript. KYC had played a vital role in assisting HJQ in the experimental work and data analysis as well as in revising and approving the submission of the final manuscript for publication. Both authors read and approved the final manuscript.

Authors' information

HJQ received his MSc degree in 2010 from Universiti Sains Malaysia, Penang, Malaysia, where he is currently working on a PhD degree in Materials Engineering in the School of Materials and Mineral Resources Engineering. KYC received his PhD degree from the School of Microelectronic Engineering, Griffith University, Brisbane, Australia, in 2004. He is currently an associate professor with Universiti Sains Malaysia, Penang, Malaysia.

Acknowledgments

One of the authors (HJQ) would like to acknowledge Universiti Sains Malaysia, The USM RU-PRGS (8044041), and The Universiti Sains Malaysia Vice Chancellor's Award for their financial support.

Received: 16 December 2012 Accepted: 20 January 2013
Published: 29 January 2013

References

1. Huang W, Khan T, Chow TP: **Enhancement-mode n-channel GaN MOSFETs on p and n-GaN/sapphire substrates.** *IEEE Electron Device Lett* 2006, **27:**796–798.
2. Chang SJ, Wang CK, Su YK, Chang CS, Lin TK, Ko TK, Liu HL: **GaN MIS capacitors with photo-CVD SiN_xO_y insulating layers.** *J Electrochem Soc* 2005, **152:**G423–G426.
3. Chang YC, Chang WH, Chiu HC, Tung LT, Lee CH, Shiu KH, Hong M, Kwo J, Hong JM, Tsai CC: **Inversion-channel GaN metal-oxide-semiconductor field-effect transistor with atomic-layer-deposited Al_2O_3 as gate dielectric.** *Appl Phys Lett* 2008, **93:**053504-1–053504-3.
4. Li S, Ware ME, Wu J, Kunets VP, Hawkridge M, Minor P, Wang Z, Wu Z, Jiang Y, Salamo GJ: **Polarization doping: reservoir effects of the substrate in AlGaN graded layers.** *J Appl Phys* 2012, **112:**053711-1–053711-5.
5. Li S, Ware M, Wu J, Minor P, Wang Z, Wu Z, Jiang Y, Salamo GJ: **Polarization induced pn-junction without dopant in graded AlGaN coherently strained on GaN.** *Appl Phys Lett* 2012, **101:**122103-1–122103-3.
6. Quah HJ, Cheong KY, Hassan Z: **Forthcoming gallium nitride based power devices in prompting the development of high power applications.** *Mod Phys Lett B* 2011, **25:**77–88.
7. Quah HJ, Cheong KY, Hassan Z, Lockman Z: **Effect of postdeposition annealing in oxygen ambient on gallium-nitride-based MOS capacitors with cerium oxide gate.** *IEEE Trans Electron Dev* 2011, **58:**122–131.
8. Cheong KY, Moon JH, Kim HJ, Bahng W, Kim NK: **Current conduction mechanisms in atomic-layer-deposited HfO_2/nitrided SiO_2 stacked gate on 4H silicon carbide.** *J Appl Phys* 2008, **103:**084113-1–084113-8.
9. Nakano Y, Jimbo T: **Interface properties of thermally oxidized n-GaN metal-oxide-semiconductor capacitors.** *Appl Phys Lett* 2003, **82:**218–220.
10. Nakano Y, Kachi T, Jimbo T: **Electrical properties of thermally oxidized p-GaN metal-oxide-semiconductor diodes.** *Appl Phys Lett* 2003, **82:**2443–2445.
11. Readinger ED, Wolter SD, Waltemyer DL, Delucca M, Mohney SE, Prenitzer BI, Giannuzzi LA, Molnar RJ: **Wet thermal oxidation of GaN.** *J Electron Mat* 1999, **28:**257–260.
12. Lin LM, Luo Y, Lai PT, Lau KM: **Influence of oxidation and annealing temperatures on quality of Ga_2O_3 film grown on GaN.** *Thin Solid Films* 2006, **515:**2111–2115.
13. Zhou Y, Ahyi C, Smith TI, Bozack M, Tin C, Williams J, Park M, Cheng A, Park J, Kim D, Wang D, Preble EA, Hanser A, Evans K: **Formation, etching and electrical characterization of a thermally grown gallium oxide on the Ga-face of a bulk GaN substrate.** *Solid State Electron* 2008, **52:**756–764.
14. Reddy VR, Reddy MSP, Lakshmi BP, Kumar AA: **Electrical characterization of Au/SiO_2/n-GaN metal-insulator-semiconductor structures.** *J Alloys Compd* 2011, **31:**8001–8007.
15. Arulkumaran S, Egawa T, Ishikawa H, Jimbo T, Umeno M: **Investigation of SiO_2/n-GaN and Si_3N_4/n-GaN insulator-semiconductor interfaces with low interface state density.** *Appl Phys Lett* 1998, **73:**809–811.
16. Chang SJ, Su YK, Chiou YZ, Chiou JR, Huang BR, Chang CS, Chen JF: **Deposition of SiO_2 layers on GaN by photochemical vapor deposition.** *J Electrochem Soc* 2003, **150:**C77–C80.
17. Chiou YZ, Su YK, Chang SJ, Gong J, Chang CS, Liu SH: **The properties of photo chemical-vapor deposition SiO_2 and its application in GaN metal-insulator semiconductor ultraviolet photodetectors.** *J Electron Mater* 2003, **32:**395–399.
18. Lee M, Ho C, Zeng J: **Electrical properties of liquid phase deposited SiO_2 on photochemical treated GaN.** *Electrochem Solid-State Lett* 2008, **11:**D9–D12.
19. Wu HR, Lee KW, Nian TB, Chou DW, Wu JJH, Wang YH, Houng MP, Sze PW, Su YK, Chang SJ, Ho CH, Chiang CI, Chern YT, Juang FS, Wen TC, Lee WI, Chyi JI: **Liquid phase deposited SiO_2 on GaN.** *Mater Chem Phys* 2003, **80:**329–333.
20. Quah HJ, Cheong KY, Hassan Z, Lockman Z: **MOS characteristics of metallorganic-decomposed CeO_2 spin-coated on GaN.** *Electrochem Solid-State Lett* 2010, **13:**H116–H118.
21. Quah HJ, Cheong KY, Hassan Z, Lockman Z: **Effects of N_2O postdeposition annealing on metal-organic decomposed CeO_2 gate oxide spin-coated on GaN substrate.** *J Electrochem Soc* 2011, **158:**H423–H432.
22. Chang YC, Chiu HC, Lee YJ, Huang ML, Lee KY, Hong M, Chiu YN, Kwo J, Wang YH: **Structural and electrical characteristics of atomic layer deposited high k HfO_2 on GaN.** *Appl Phys Lett* 2007, **90:**232904-1–232904-3.
23. Kim J, Gila BP, Mehandru R, Johnson JW, Shin JH, Lee KP, Luo B, Onstine A, Abernathy CR, Pearton SJ, Ren F: **Electrical characterization of GaN metal-oxide-semiconductor diodes using MgO as the gate oxide.** *J Electrochem Soc* 2002, **149:**G482–G484.
24. Liu C, Chor EF, Tan LS, Dong Y: **Structural and electrical characterizations of the pulsed-laser-deposition-grown Sc_2O_3/GaN heterostructure.** *Appl Phys Lett* 2006, **88:**222113-1–222113-3.
25. Quah HJ, Cheong KY: **Study on gallium nitride-based metal-oxide-semiconductor capacitors with RF magnetron sputtered Y_2O_3 gate.** *IEEE Trans Electron Dev* 2012, **59:**3009–3016.

26. Chang WH, Lee CH, Chang P, Chang YC, Lee YJ, Kwo J, Tsai CC, Hong JM, Hsu CH, Hong M: **High k dielectric single-crystal monoclinic Gd_2O_3 on GaN with excellent thermal, structure, and electrical properties.** *J Cryst Growth* 2009, **311:**2183–2186.
27. Chang WH, Chang P, Lee WC, Lai TY, Kwo J, Hsu CH, Hong JM, Hong M: **Epitaxial stabilization of a monoclinic phase in Y_2O_3 films on c-plane GaN.** *J Cryst Growth* 2011, **323:**107–110.
28. Quah HJ, Lim WF, Cheong KY, Hassan Z, Lockman Z: **Comparison of metal-organic decomposed (MOD) cerium oxide (CeO_2) gate deposited on GaN and SiC substrates.** *J Crys Growth* 2011, **326:**2–8.
29. Quah HJ, Cheong KY: **Deposition and post-deposition annealing of thin Y_2O_3 film on n-type Si in argon ambient.** *Mat Chem Phys* 2011, **130:**1007–1015.
30. Quah HJ, Cheong KY: **Effects of post-deposition annealing ambient on Y_2O_3 gate deposited on silicon by RF magnetron sputtering.** *J Alloys Compd* 2012, **529:**73–83.
31. Robertson J, Falabretti B: **Band offsets of high K gate oxides on III-V semiconductors.** *J Appl Phys* 2006, **100:**014111-1–014111-8.
32. Li S, Han L, Chen Z: **The interfacial quality of HfO_2 on silicon with different thicknesses of the chemical oxide interfacial layer.** *J Electrochem Soc* 2010, **157:**G221–G224.
33. Rastogi AC, Sharma RN: **Interfacial charge trapping in extrinsic Y_2O_3/SiO_2 bilayer gate dielectric based MIS devices on Si(100).** *Semicond Sci Technol* 2011, **16:**641–650.
34. Kraut EA, Grant RW, Waldrop JR, Kowalczyk SP: **Semiconductor core-level to valence-band maximum binding-energy differences: precise determination by X-ray photoelectron spectroscopy.** *Phys Rev B* 1983, **28:**1965–1977.
35. Kraut EA, Grant RW, Waldrop JR, Kowalczyk SP: **Precise Determination of the valence-band edge in X-ray photoemission spectra: application to measurement of semiconductor interface potentials.** *Phys Rev Lett* 1980, **44:**1620–1623.
36. Miyazaki S: **Characterization of high-k gate dielectric/silicon interfaces.** *Appl Surf Sci* 2002, **190:**66–74.
37. Wang XJ, Liu M, Zhang LD: **Temperature dependence of chemical states and band alignments in ultrathin HfO_xN_y/Si gate stacks.** *J Phys D: Appl Phys* 2012, **45:**335103-1–335103-5.
38. Umezawa N, Shiraishi K, Ohno T, Watanabe H, Chikyow T, Torii K, Yamabe K, Yamada K, Kitajima H, Arikado T: **First-principle studies of the intrinsic effect of nitrogen atoms on reduction in gate leakage current through Hf-based high-k dielectrics.** *Appl Phys Lett* 2005, **86:**143507-1–143507-3.
39. Quah HJ, Lim WF, Wimbush SC, Lockman Z, Cheong KY: **Electrical properties of pulsed laser deposited Y_2O_3 gate oxide on 4H-SiC.** *Electrochem Solid-State Lett* 2010, **13:**H396–H398.
40. Schroder DK: *Semiconductor Material and Device Characterization*. New York: Wiley; 1998.
41. Jinesh KB, Lamy Y, Tois E, Besling WFA: **Charge conduction mechanisms of atomic-layer-deposited Er_2O_3 thin films.** *Appl Phys Lett* 2009, **94:**252906-1–252906-3.
42. Kohl AS, Conforto AB, Z'Graggen WJ, Lang A: **An integration transcranial magnetic stimulation mapping technique using non-linear curve fitting.** *J Neurosci Meth* 2006, **157:**278–284.
43. Kumar KV: **Pseudo-second order models for the adsorption of safranin onto activated carbon: comparison of linear and non-linear regression methods.** *J Hazard Mater* 2007, **142:**564–567.

doi:10.1186/1556-276X-8-53
Cite this article as: Quah and Cheong: **Effects of post-deposition annealing ambient on band alignment of RF magnetron-sputtered Y_2O_3 film on gallium nitride.** *Nanoscale Research Letters* 2013 **8**:53.